Supporting information for

Ultrathin $NiCo_2O_4$ Nanosheets with Dual-Metal Active Sites for Enhanced Solar Water Splitting of $BiVO_4$ Photoanode

Chenchen Feng[a,b], Qi Zhou[c], Bin Zheng[c], Xiang Cheng[a,b] , Yajun Zhang[a] and Yingpu Bi[a]*

[a] State Key Laboratory for Oxo Synthesis & Selective Oxidation, National Engineering Research Center for Fine Petrochemical Intermediates, Lanzhou Institute of Chemical Physics, CAS, Lanzhou 730000, Gansu, China.

E-mail: yingpubi@licp.cas.cn

[b] University of Chinese Academy of Sciences, Beijing 100049, China.

[c] College of Materials Science and Engineering, Lanzhou University of Technology, Lanzhou 730050, Gansu, China.

Experimental section

Preparation of nanoporous Mo:$BiVO_4$ photoanodes:

Our work about preparation of nanoporous $BiVO_4$ photoanodes have been published.[1,2] In a typical procedure, nanoporous Mo:$BiVO_4$ photoanodes were also fabricated by drop-casting the precursor solution on FTO substrates. FTO substrates were cleaned under sonication by sequentially immersing in acetone, isopropanol, ethanol and distilled water, and then immersed in the H_2SO_4/H_2O_2 (3:1, volume ratio) solution for one hour to make them uniformly hydrophilic. In detail, the preparation of precursor solution will be shown as the following. At first, 0.272 g polyethylene glycol 600 (PEG-600), 1.2 mmol $Bi(NO_3)_3{\cdot}5H_2O$, 1.1765 mmol NH_4VO_3 and 0.0034 mmol $(NH_4)_6Mo_7O_{24}{\cdot}4H_2O$ were dissolved orderly in ethylene glycol. After continuous ultrasonic for a few hours, a yellow transparent precursor solution can be obtained. Then, 0.2 mL precursor solution was drop-cast on FTO substrates (1×5 cm^2), The sample was dried in an oven at 150 °C for 60 min and then annealed in a muffle furnace in air at 500 °C for 2.5 hours. Finally, a yellow $BiVO_4$ photoanode would generate on the FTO substrates. Of course, the pure $BiVO_4$ photoanode was prepared without adding $(NH_4)_6Mo_7O_{24}{\cdot}4H_2O$. The samples were denoted as $BiVO_4$ and Mo:$BiVO_4$.

Preparation of ultrathin $NiCo_2O_4$ nanosheets:

Ultrathin $NiCo_2O_4$ nanosheets were fabricated by a special dealloying method. The powders of Ni, Co, Al (atomic ratio = 1.7:3.3:95) were uniformly mixed via ball-milling. These mixed powders were processed into raw material (diameter = 15 mm) by cold press molding technology, and the raw materials were calcined using a high-frequency induction furnace in vacuum to fabricate alloy ingots (Ni, Co, Al). After rapid solidification, alloy ingots turned into alloy ribbons (wide = 4~6 mm, thickness = 20~40 μm). In order to remove Al metal, alloy ribbons were immersed in a 25 wt% NaOH aqueous solution. The dealloying was performed at 65 °C for 30 h. The as-dealloyed samples were rinsed using distilled water and dried at room temperature in vacuum. Finally, the as-prepared nanoporous Ni-Co alloy were annealed at 350 °C in air for 2 h with a ramping rate of 2 °C/min to obtain ultrathin mesoporous $NiCo_2O_4$ nanosheets.

Preparation of bulk $NiCo_2O_4$:

0.2 mmol of $Ni(NO_3)_2 \cdot 6H_2O$, 0.4 mmol of $Co(NO_3)_2 \cdot 6H_2O$, 0.5 mmol of hexamethylenetetramine (HMT) and 0.05 mmol of trisodium citrate dihydrate (TSC) were added into the 40 mL of deionized (DI) water. Then the mixed solution was refluxed with rigorous stirring in an oil bath at 90 °C for 6 h. After cooling down to room temperature naturally, the black precipitate was harvested by centrifugation and washed with DI water and ethanol for several times. Finally, the obtained product of Ni-Co precursor was dried overnight at 80 °C and further annealed at 300 °C for 3 h in air with a heating rate of 2 °C min^{-1} to obtain crystalline $NiCo_2O_4$.

Preparation of $NiCo_2O_4$/Mo:$BiVO_4$ photoanodes:

The $NiCo_2O_4$ modified nanoporous Mo: $BiVO_4$ were prepared by spin-coating $NiCo_2O_4$ precursor solutions (0.5 mg/mL) at a fixed rotation speed of 800 rpm for 60 seconds and 3000 rpm for 30 seconds on Mo:$BiVO_4$ photoanodes. After spin-coating, $NiCo_2O_4$/Mo:$BiVO_4$ electrodes were dried at room temperature. Finally, the as-prepared specimens were heated at 350°C for 120 min in air.

Preparation of NiO nanosheets:

Firstly, the Ni-based nanosheets precursor was prepared using a modified method which was reported by previous literature.[3] In a typical run, 4 mmol nickel acetate and 8 mmol hexamethylenetetramine (HMT) were dissolved in 35 mL of distilled water under vigorous stirring for 30 min to form a transparent solution. The mixture was transferred into a 40 mL Teflon-lined

autoclave, sealed and heated at 120 °C for 12 h. Next, the autoclave was allowed to cool down to room temperature, and the final product was collected by centrifuging the mixture, washed with water and ethanol for several times. Secondly, in order to prepare NiO nanosheets, 500 mg of Ni-based precursor was placed in a crucible. Then the muffle furnace was heated to 500 °C with a rate of 10 °C min^{-1} in air and maintained for 3 h. The final products were collected for further characterization.

Preparation of Co_3O_4 nanoparticles:

The Co_3O_4 nanoparticles was synthesized according to a previously reported procedure.[4] In brief, after 0.125 g $Co(CH_3COO)_2 \cdot 4H_2O$ was dissolved in 50 mL distilled water, 0.8 mL ammonium solution ($NH_3 \cdot H_2O$, 25 wt%) was added into solution, followed by stirring for 30 min. Then the solution was transferred to a 100 mL Teflon-lined stainless-steel autoclave, treated at 150 °C for 3 h. After the stainless autoclave was cooled to room temperature by flowing water, the obtained products were centrifuged, washed with deionized water and ethanol for a few times, respectively. Lastly, the obtained samples were dried at 80 °C.

Preparation of NiO/Mo:$BiVO_4$ and Co_3O_4/Mo:$BiVO_4$ photoanodes:

The NiO and Co_3O_4 modified nanoporous Mo:$BiVO_4$ photoanodes were prepared by drop-coating and thermal treating method. In a typical procedure, NiO (2.5 mM) and Co_3O_4 (1.7 mM) precursor solutions (0.1 mL) were respectively drop-coated onto the Mo:$BiVO_4$ electrodes. Then composites were fully dried at 80 °C for 10 min and annealed at 350 °C for 120 min in air. The samples were respectively denoted as NiO/Mo:$BiVO_4$ and Co_3O_4/Mo:$BiVO_4$.

Characterization.

The X-ray diffraction spectra (XRD) measurements were performed on a Rigaku RINT-2000 instrument utilizing Cu Kα radiation (40 KV). The XRD patterns were recorded from 10° to 90° with a scanning rate of 0.067°/s. Scanning electron microscopy (SEM) measurements were carried out on a field-emission scanning electron microscope (JSM-6701F. JEOL) operated at an accelerating voltage of 5 KV. Transmission electron microscopy (TEM) measurements were carried out by using a FEI Tecnai TF20 microscope operated at 200 kV. UV-vis diffuse reflectance spectra were taken on an UV-2550 (Shimadzu) spectrometer by using $BaSO_4$ as the reference. Photoluminescence spectra and time-resolved photoluminescence spectra were monitored by LP 980 laser flash photolysis instrument (Edinburgh, U.K.). Atomic force microscopy (AFM) was

recorded by Bruker Dimension Icon AFM system and a Veeco Nanoscope IVa Multimode system.

Photoelectrochemical measurements.

The Photoelectrochemical properties were measured by an electrochemical analyzer (CHI660D) in a standard three-electrode system with a working electrode, a Pt foil as the counter electrode, and a saturated Ag/AgCl (4 M KCl) as a reference electrode. The photoanodes as the working electrode. The illumination source was a 300 W Xe arc lamp (Beijing Perfectlight Technology Co. Ltd., Microsolar 300 UV) equipped with an AM 1.5G filter, and the power intensity of the incident light was calibrated to 100 mW/cm^2 at the surface of the working electrode. The current-voltage (*J-V*) characteristic of the electrodes, with a scan rate of 10 mV/s. Illumination through the FTO side (back-side illumination) was used. A 0.5 M potassium phosphate (KH_2PO_4) buffer solution (pH=7) was used as the electrolyte. All potentials of the working electrode were presented against the reversible hydrogen electrode (RHE). The conversion between potentials vs. Ag/AgCl and vs. RHE is performed using the equation below.

$$E_{RHE} = E_{Ag/AgCl} + E_{Ag/AgCl}\,(reference) + 0.0591 \times pH$$

($E_{Ag/AgCl}$ (reference) = 0.1976 V vs. NHE at 25 °C)

Where pH is a pH value of the electrolyte.

According to the Mott-Schottky curves, charge carrier density (N_d) can be calculated using the following equation:

$$N_d = \frac{2}{e\varepsilon_0\varepsilon} \times \left(\frac{d\left(\frac{1}{C^2}\right)}{dV_s} \right)^{-1}$$

The electronic charge (e) is 1.6×10^{-19} C, vacuum permittivity (ε_0) is 8.86×10^{-12} F m^{-1}, and relative permittivity (ε) is 68 for $BiVO_4$.[5] C (F cm^{-2}) is the space charge capacitance in the semiconductor (obtained from Mott-Schottky curves), and V_s (V) is the applied potential for MS curves.

The incident photon to current efficiency (IPCE) was determined using a solar simulator (Beijing Perfectlight Technology Co. Ltd., PLS-SXE 300C) and monochromator (Beijing NBeT, 71SW 302). Power density of monochromatic light (300 nm - 800 nm) tested by a monochromator (Beijing NBeT, 71SW 302), optical power and energy meter (THORLABS, PM320E) and slim photodiode power sensor (THORLABS, S130VC). IPCE was measured at 0.6 V vs. RHE in 0.5 M KH_2PO_4 buffer solution (pH 7) using the same three-electrode setup described above for

photocurrent measurements. IPCE was calculated as follows:

$$IPCE = \frac{1240 \times I(mA/cm^2)}{P_{light}(mW/cm^2) \times \lambda\ (nm)}$$

Where I is the measured photocurrent density at a specific wavelength, λ is the wavelength of incident light and P_{light} is the measured light power density at that wavelength.

Supposing 100% Faradaic efficiency, the applied bias photon-to-current efficiency (ABPE) was calculated by following equation:

$$ABPE(\%) = \frac{I(mA/cm^2) \times (1.23 - V_{bias})(V)}{P_{light}(mW/cm^2)} \times 100$$

Where I is the photocurrent density from the J-V curves shown in Figure 3A, V_{bias} is the applied bias between WE and RHE, P_{light} is the incident illumination power density (100 mW cm^{-2}).

The electrochemical impedance spectroscopy (EIS) Nyquist plots were obtained at 1.23 V vs. RHE with small AC amplitude of 10 mV in the frequency range of 10^{-2} to 10^5 Hz under AM 1.5G illumination (100 mW cm^{-2}). The measured spectra were fitted with Z-view.

Detection of the amount of hydrogen and oxygen evolution:

To quantitatively determine the amount of H_2 and O_2 produced from the overall water splitting, an online gas analysis system (Labsolar 6A, Beijing Perfectlight Technology Co. Ltd.) and a gas chromatograph (GC 7890A, Agilent Technologies) were employed. The produce of H_2 and O_2 was performed in a three-electrode system at a constant bias of 1.23 V vs. RHE under AM 1.5G illumination (100 mW cm^{-2}).

The Faradaic efficiency for PEC water splitting has been calculated based on the following equation:

$$FE(\%) = \frac{A \times n(mol) \times F(C\ mol^{-1})}{Charge\ passed\ through\ WE\ (C)} \times 100$$

where n is moles of evolved H_2 or O_2 gas, A is the number of electrons required to generate one H_2 or O_2 molecule (two for H_2, four for O_2) and F is the Faraday constant (96485.33 C mol^{-1}).

Electrochemical measurements:

The catalyst slurry was prepared by mixing the catalyst (10 mg), 5 % Nafion (0.08 mL), ethanol (0.5 mL), and DI water (0.5 mL). Drop casting was employed to fabricate the electrodes wherein the slurry was deposited onto 1×2 cm^2 nickel foam (NF). Electrolysis experiments were performed

in a standard three-electrode cell, which was composed of working electrode, counter electrode (Pt foil) and reference electrode (Ag/AgCl, sat. KCl). 1 M KOH was used as the electrolyte. The OER properties were performed from 0 to 1.4 V vs. Ag/AgCl with a scan rate of 50 mV s^{-1}. *iR* correction was applied where the electrode and solution resistance were determined by applying impendence measurement. The electrochemical impedance spectroscopy (EIS) Nyquist plots were obtained at 1.4 V vs. Ag/AgCl with small AC amplitude of 5 mV in the frequency range of 10^{-1} to 10^{5} Hz under dark. The measured spectra were fitted with Z-view.

Supplemental Figures

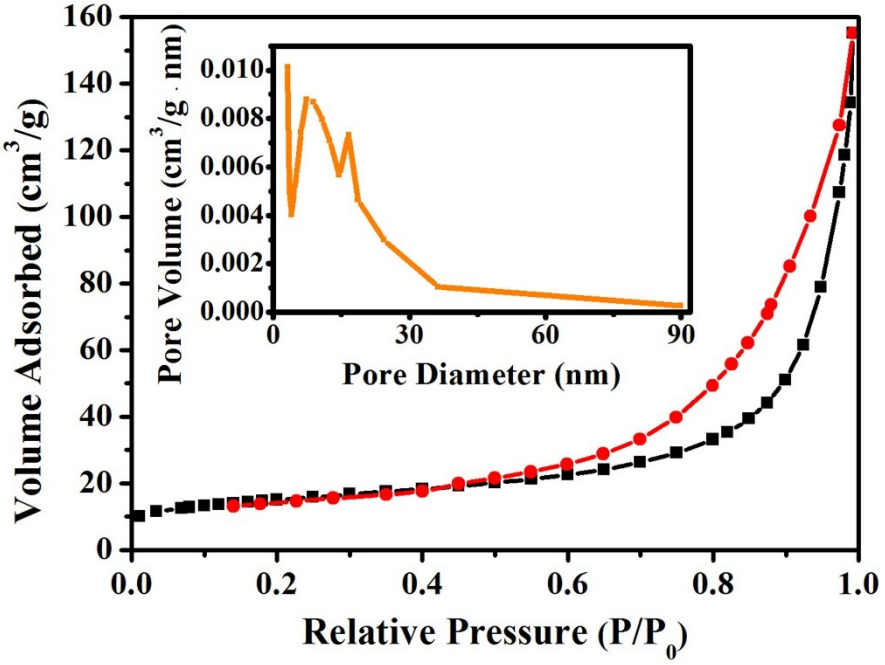

Figure S1. N_2 adsorption-desorption isotherm of the ultrathin $NiCo_2O_4$ nanosheets. (Inset) Corresponding pore size distribution curve calculated from the desorption branch of the N_2 isotherm by the Barrett-Joyner-Halenda (BJH) formula.

Additional discussion:

As shown in Figure S1, a type IV N_2 adsorption isotherm with a type H1 hysteresis loop was observed. This result indicates that the sample possesses a mesoporous feature.

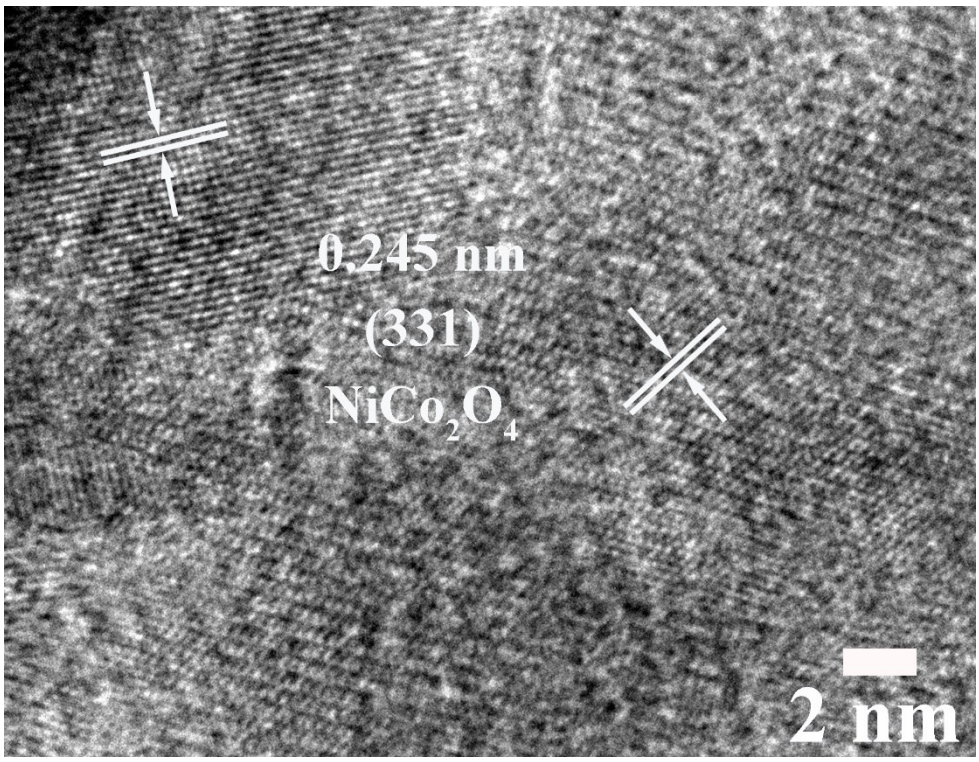

Figure S2. HR-TEM image of the ultrathin $NiCo_2O_4$ nanosheets.

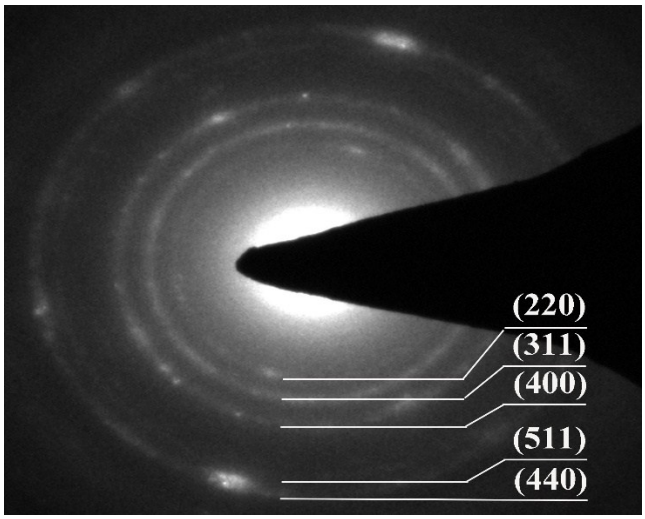

Figure S3. SAED image of the ultrathin $NiCo_2O_4$ nanosheets.

Additional discussion:

In addition, the crystal structure of the ultrathin $NiCo_2O_4$ nanosheets were further studied by selected-area electron diffraction (SAED, Figure S3). The SAED pattern shows a series of Debye-Scherrer diffraction rings, suggesting their polycrystalline characteristics.

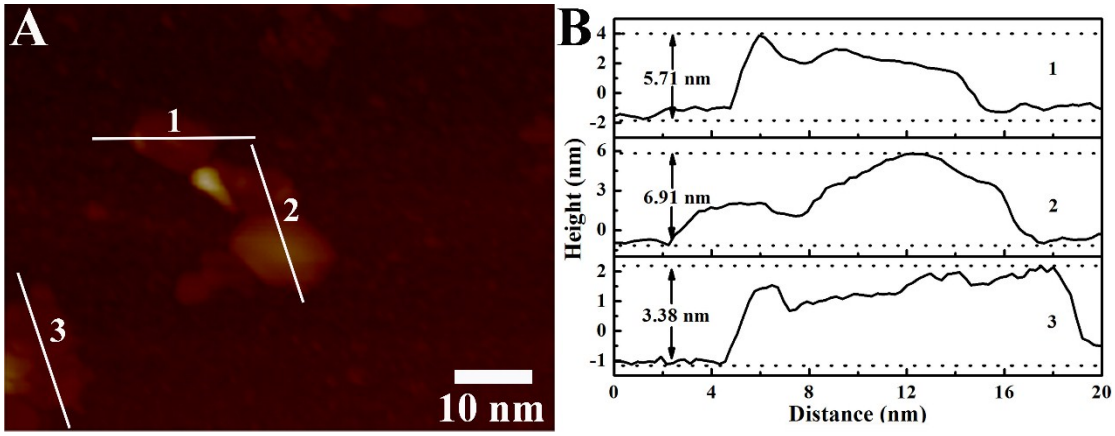

Figure S4. (A) AFM image and (B) corresponding height profile of the ultrathin $NiCo_2O_4$ nanosheets.

Additional discussion:

The thickness of the as-prepared $NiCo_2O_4$ nanosheets was further studied by atomic force microscopy (AFM). As shown in Figure S4**,** the height of the nanosheets ranges from 3-7 nm.

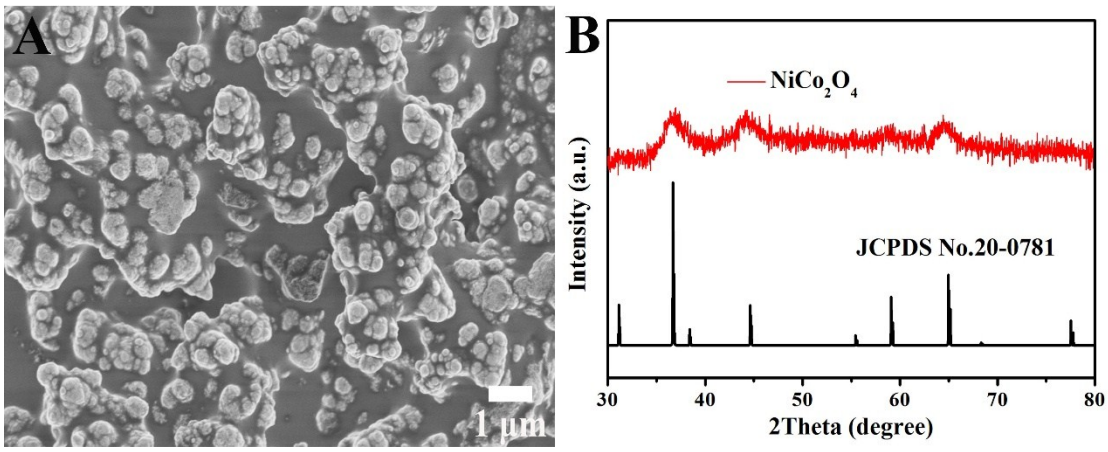

Figure S5. SEM image and XRD pattern of bulk $NiCo_2O_4$.

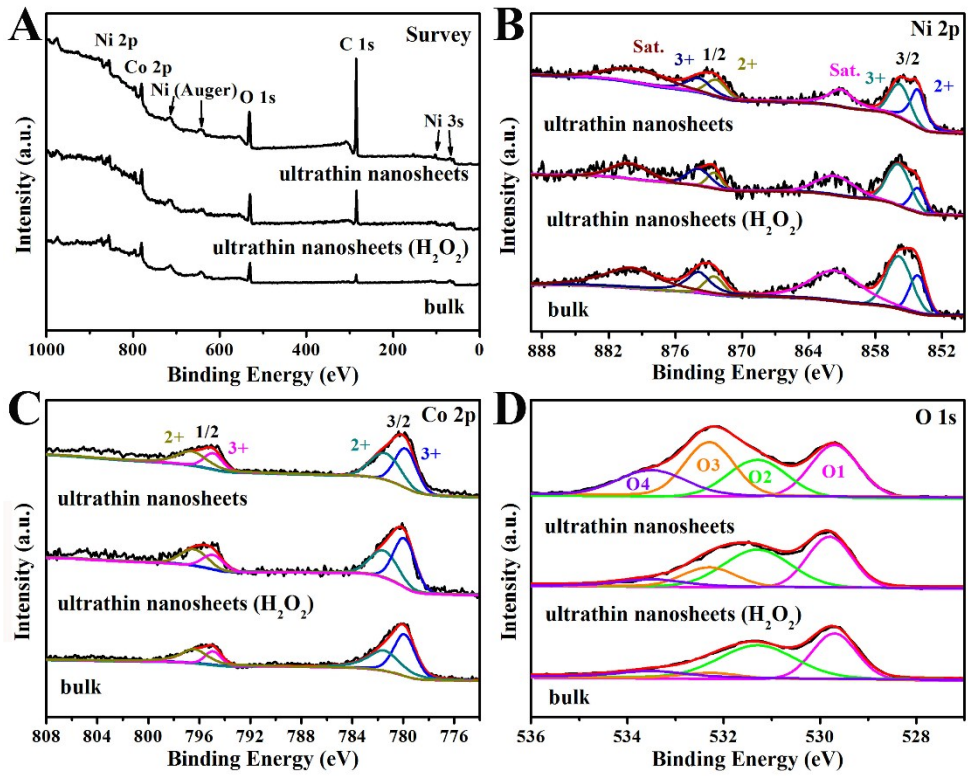

Figure S6. XPS spectra of survey (A), Ni 2p (B), Co 2p (C) and O 1s (D) for the ultrathin $NiCo_2O_4$ nanosheet with/without H_2O_2 treatment and bulk $NiCo_2O_4$.

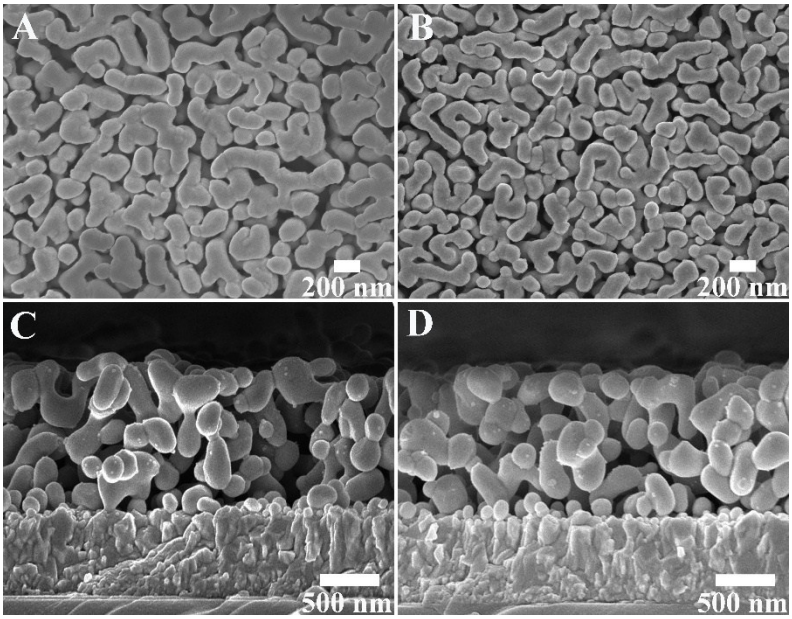

Figure S7. (A, B) Top and (C, D) side-view SEM images of $BiVO_4$ (left) and Mo:$BiVO_4$ (right) photoanode, respectively.

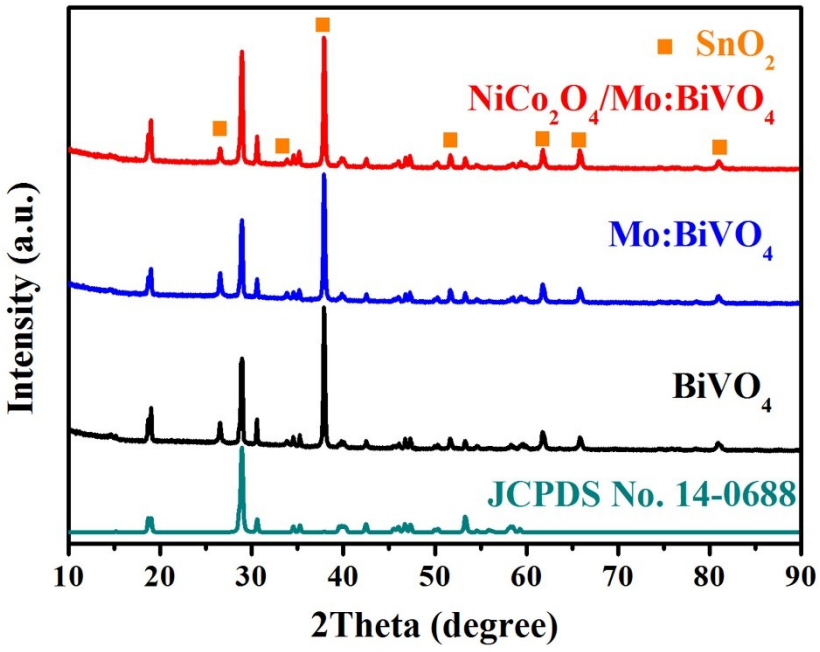

Figure S8. XRD patterns of $BiVO_4$, Mo:$BiVO_4$ and $NiCo_2O_4$/Mo:$BiVO_4$ photoanodes.

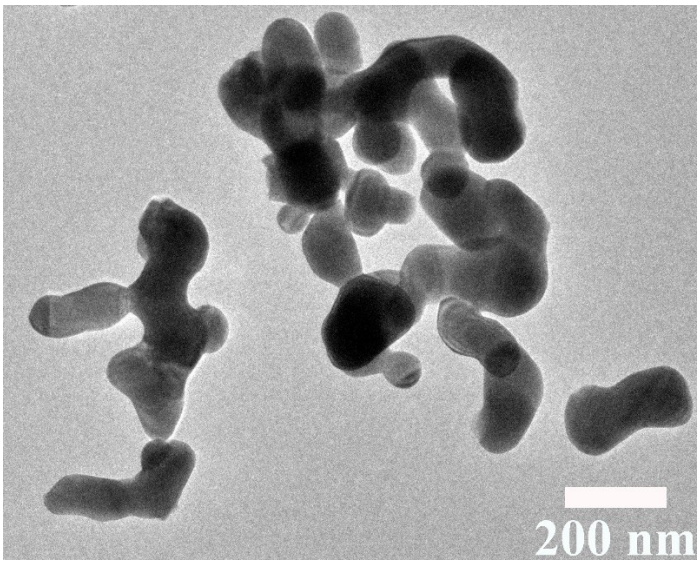

Figure S9. TEM image of $NiCo_2O_4$/Mo:$BiVO_4$.

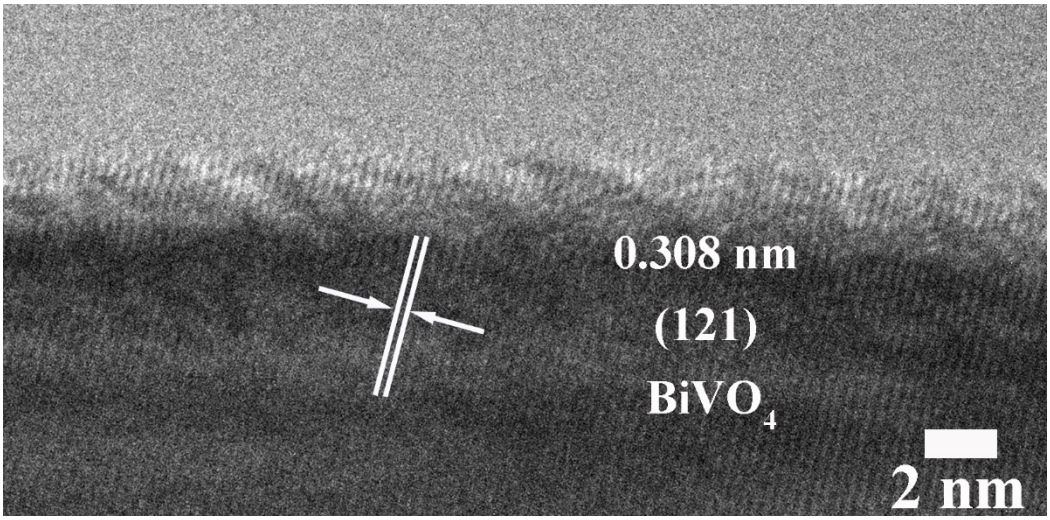

Figure S10. HR-TEM image of Mo:$BiVO_4$.

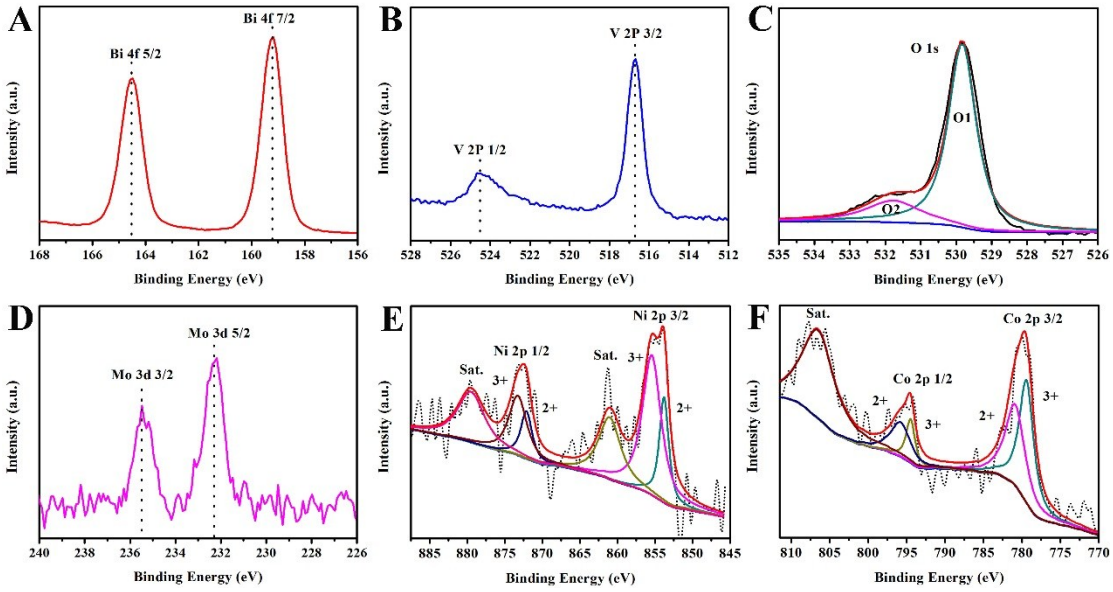

Figure S11. XPS spectra of $NiCo_2O_4$/Mo:$BiVO_4$ photoanode. (A) Bi 4f, (B) V 2p, (C) O 1s, (D) Mo 3d, (E) Ni 2p and (F) Co 2p.

Additional discussion:

The XPS spectra of the $NiCo_2O_4$/Mo:$BiVO_4$ photoanodes are shown in Figure S11, which further conform the successful incorporation of $NiCo_2O_4$ and Mo:$BiVO_4$.

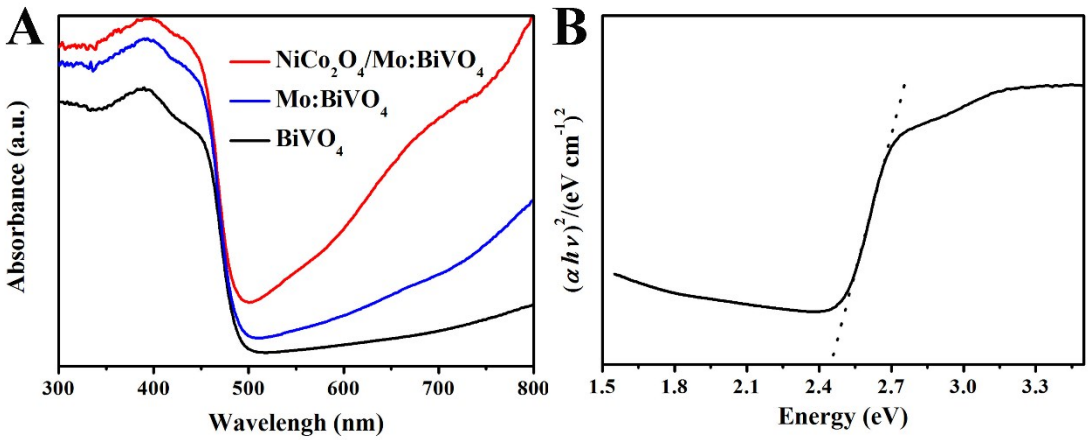

Figure S12. (A) UV-vis absorption spectrum of $BiVO_4$, Mo:$BiVO_4$ and $NiCo_2O_4$/Mo:$BiVO_4$ photoanodes, (B) the Tauc plot of $BiVO_4$.

Additional discussion:

UV-vis absorption (Figure S12) shows the similar spectral response range for the pristine $BiVO_4$ and $NiCo_2O_4$/Mo:$BiVO_4$ photoanodes, and a band up of 2.45 eV for the pristine $BiVO_4$ photoanode is consistent with recent reports.

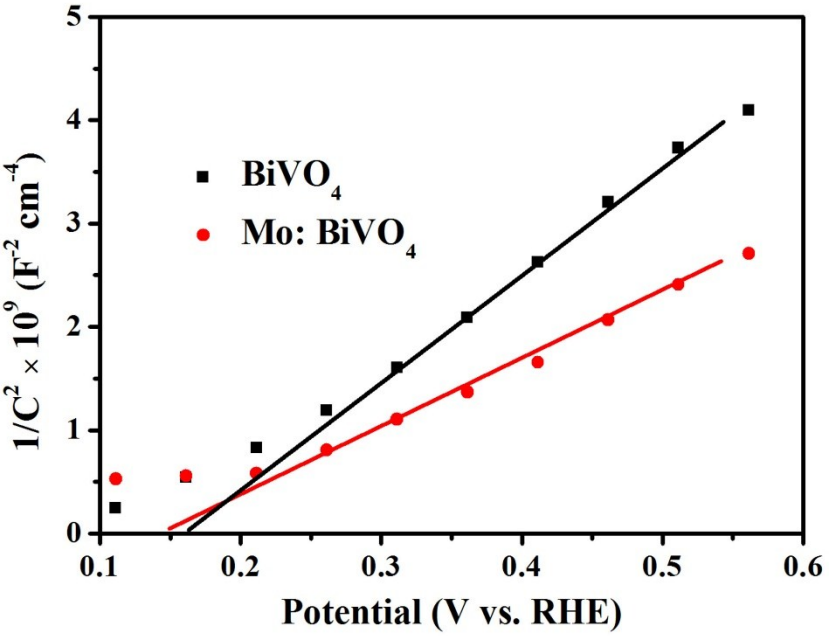

Figure S13. Mott-Schottky plots of the pristine $BiVO_4$ and Mo:$BiVO_4$ photoanodes.

Additional discussion:

To clarify the enhanced charge carrier density upon Mo^{6+} doped into the porous $BiVO_4$, Mott-Schottky analysis was conducted (Figure S13). The carrier densities calculated from the slopes of the Mott-Schottky plots for pristine $BiVO_4$ and Mo:$BiVO_4$ photoanodes are 2.02×10^{18} and 3.17×10^{18} cm^{-3}. This result suggests that Mo^{6+} doping is effective in improving the electrical conductivity of $BiVO_4$ by increasing its donor density.

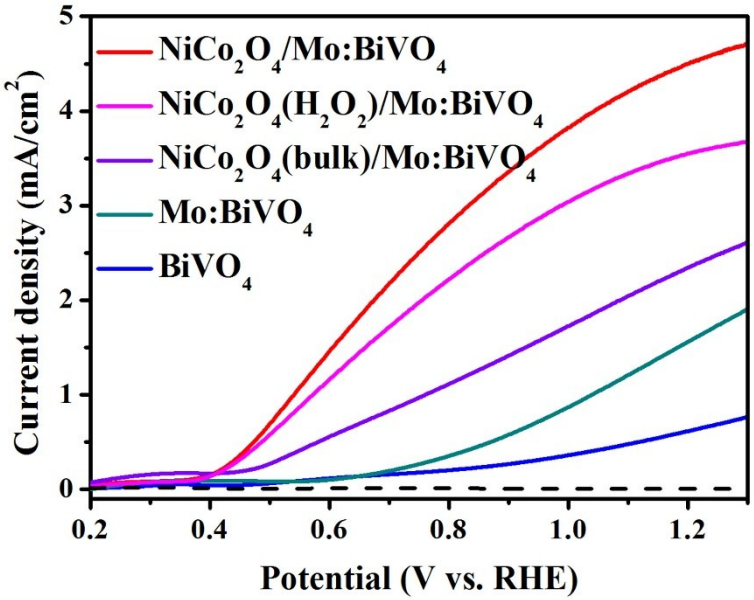

Figure S14. LSV curves of the pristine $BiVO_4$, Mo:$BiVO_4$, $NiCo_2O_4$(bulk)/Mo:$BiVO_4$, $NiCo_2O_4$ (H_2O_2)/Mo:$BiVO_4$ and $NiCo_2O_4$/Mo:$BiVO_4$ photoanodes measured in 0.5 M KH_2PO_4 (pH=7) electrolyte under AM 1.5G irradiation.

Additional discussion:

The ultrathin $NiCo_2O_4$ nanosheets (H_2O_2) with poor oxygen vacancies and bulk $NiCo_2O_4$ modified Mo:$BiVO_4$ photoanodes respectively show a drastically decreased photocurrent density of 3.6 and 2.4 mA cm^{-2} at 1.23 V_{RHE} (Figure S14). These results highlight the essential role of OER cocatalyst with ultrathin structure and oxygen vacancies on improving PEC performance.

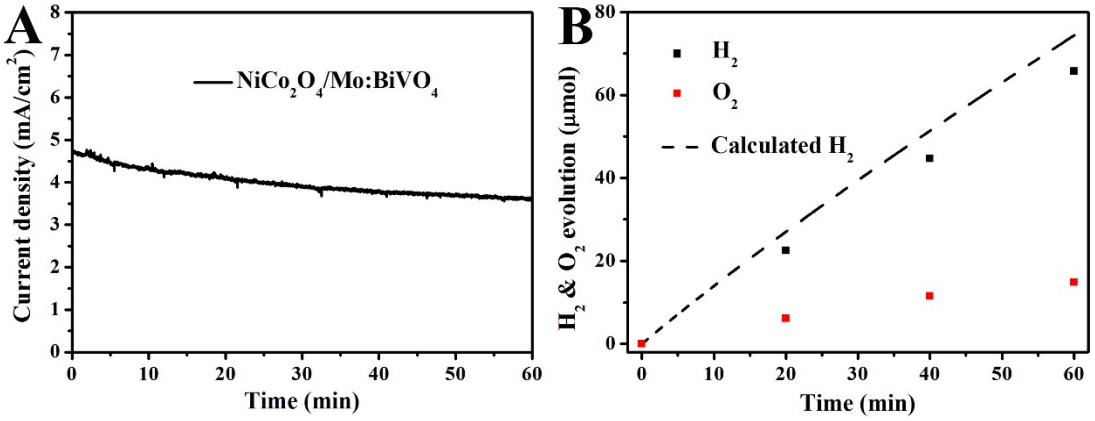

Figure S15. (A) J-t curve of $NiCo_2O_4$/Mo:$BiVO_4$ photoanode. (F) H_2 and O_2 evolution from PEC water splitting at 1.23 V_{RHE} under AM 1.5G light irradiation.

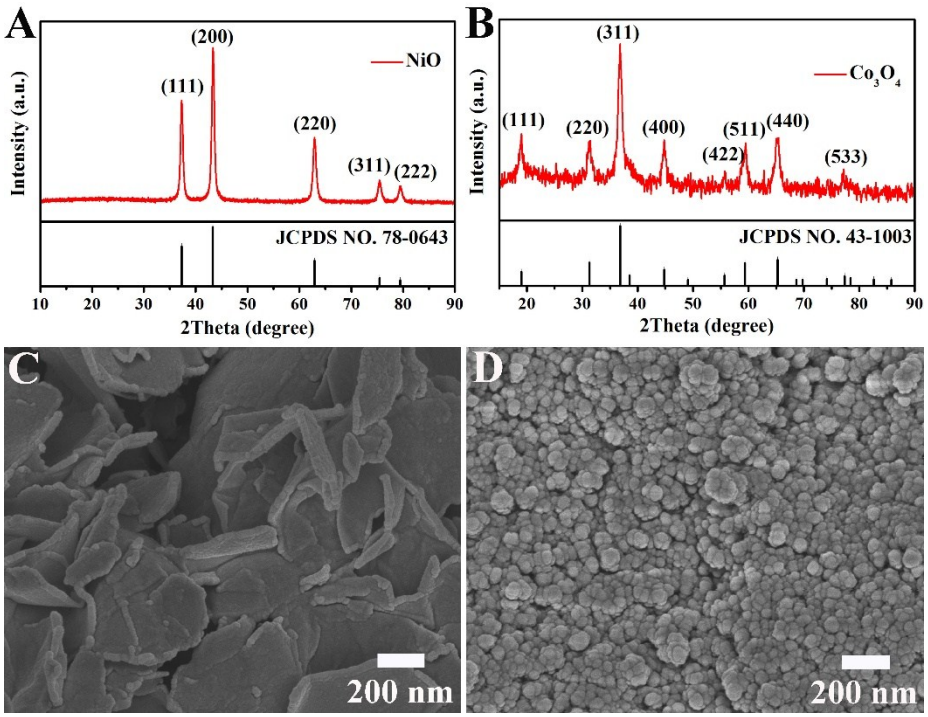

Figure S16. XRD patterns and SEM images of NiO nanosheets (A, C) and Co_3O_4 nanoparticles (B, D), respectively.

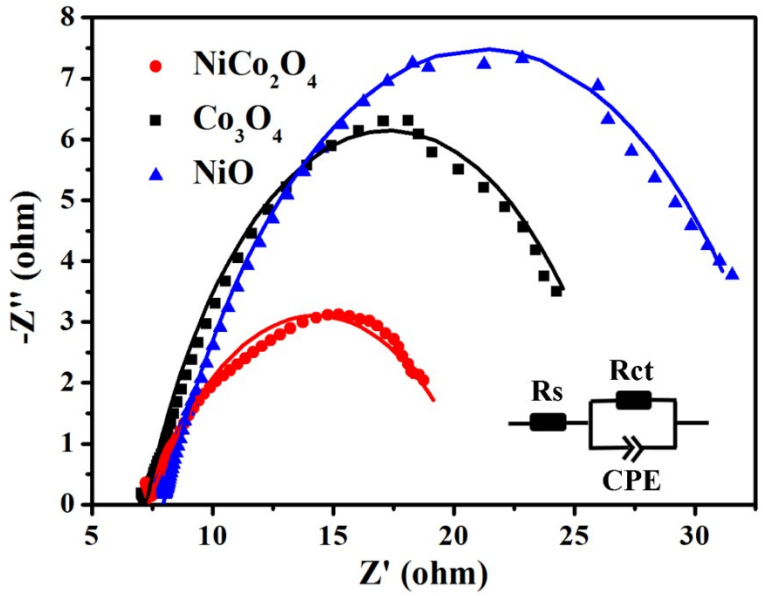

Figure S17. EIS Nyquist plots (inset is the equivalent circuit) of NiO, Co_3O_4 and $NiCo_2O_4$.

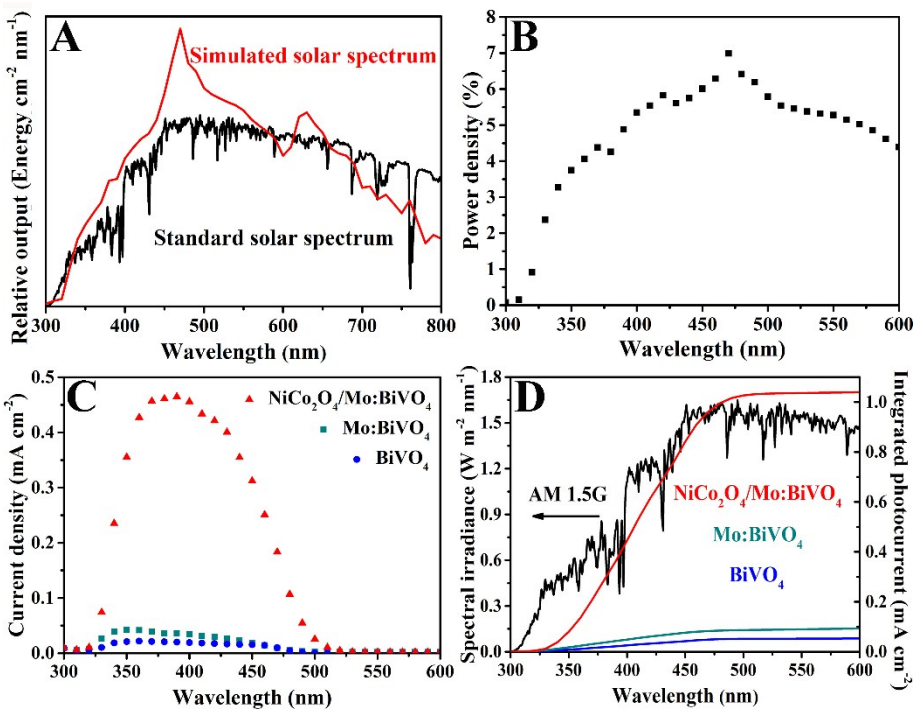

Figure S18. (A) Simulated solar spectrum and standard solar spectrum (ASTM G173-03). (B) Power density of monochromatic light in 0.5 M KH_2PO_4 (pH=7) electrolyte. (C) The monochromatic photocurrent density of photoanodes were measured at 0.6 V_{RHE}. (D) Calculated photocurrent density curves by integrating IPCE curves in (D) with the standard solar spectrum.

Additional discussion:

By integrating the IPCE over the standard AM 1.5G spectrum, photocurrent density of 1.1 mA cm^{-2} was obtained for $NiCo_2O_4$/Mo:$BiVO_4$ photoanode (Figure S18D), which is slightly lower than the value (1.4 mA cm^{-2}, at 0.6 V_{RHE}) obtained from the LSV curve (Figure 3A). This result might be due to the deviation of our solar simulator from the standard AM 1.5G spectrum (ASTM G173-03) in the absorption range of bismuth vanadate.

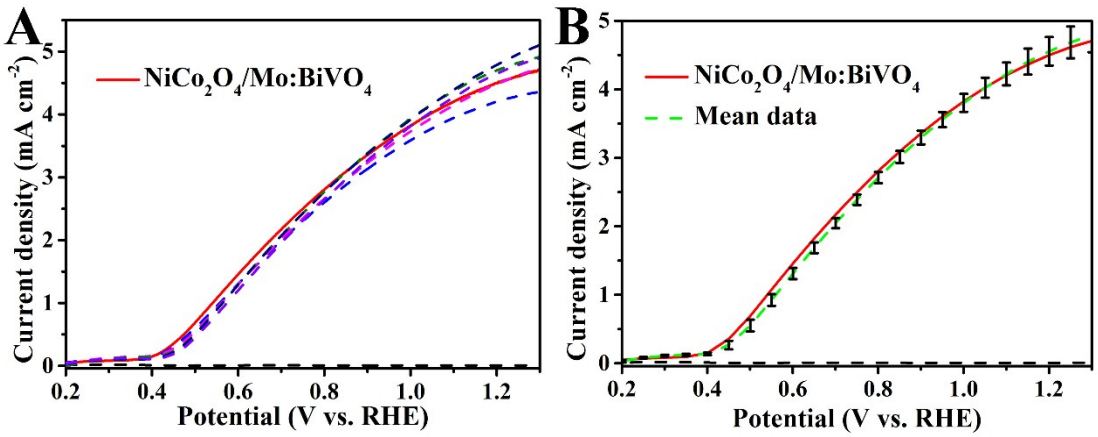

Figure S19. (A) The new LSV curves of $NiCo_2O_4$/Mo:$BiVO_4$ photoanodes. (B) The mean data with standard deviations.

Additional discussion:

The photocurrent density of $NiCo_2O_4$/Mo:$BiVO_4$ photoanodes were retested in 0.5 M KH_2PO_4 (pH=7) electrolyte under AM 1.5G irradiation (100 mW cm^{-2}). The new LSV curves (dotted lines) and the mean data with standard deviations were respectively shown in Figure S19A and Figure S19B. The new photocurrent curves are close to the one used in manuscript. This result clearly demonstrates that the PEC performance of the as-prepared photoanodes is repeatable and efficient.

Table S1. Parameters of the ultrathin $NiCo_2O_4$ nanosheets obtained from N_2 adsorption-desorption measurement.

Sample	BET (m^2/g)	Pore volume (cm^3/g)	Pore size (nm)
$NiCo_2O_4$	53.24	0.24	14.73

Table S2. The values of the elements in equivalent circuit fitted in the Nyquist plots of Figure. 3D.

Sample	Rs (Ω)	CPE 1	CPE 2	Rct (Ω)
$BiVO_4$	104.8	1.92×10^{-4}	0.686	1907
Mo: $BiVO_4$	55.83	6.26×10^{-4}	0.59	1560
$NiCo_2O_4$/Mo: $BiVO_4$	65.29	9.898×10^{-4}	0.487	138.3

Table S3. The values of the elements in equivalent circuit fitted in the Nyquist plots of Figure. S16.

Sample	Rs (Ω)	Rct (Ω)	CPE 1	CPE 2
$NiCo_2O_4$	7.33	13.86	0.02	0.537
Co_3O_4	7.2	20.13	0.012	0.698
NiO	7.9	26.46	0.007	0.656

Reference

[1] C. C. Feng, Z. B. Jiao, S. P. Li, Y. Zhang and Y. P. Bi, *Nanoscale*, 2015, **7**, 20374-20379.

[2] C. C. Feng, Z. H. Wang, Y. Ma, Y. J. Zhang, L. Wang and Y. P. Bi, *Appl. Catal. B*, 2017, **205**, 19-23.

[3] Z. H. Wang, G. J. Zou, C. C. Feng, Y. Ma, X. L. Wang and Y. P. Bi, *RSC Adv*, 2016, **6**, 83350-83355.

[4] X. X. Chang, T. Wang, P. Zhang, J. J. Zhang, A. Li and J. L. Gong, *J. Am. Chem. Soc.,* 2015, **137**, 8356-8359.

[5] S. C. Wang, P. Chen, J. H. Yun, Y. X. Hu and L. Z Wang, *Angew. Chem.,* 2017, **129**, 8620-8624.